International Research Journal of Pure & Applied Chemistry

15(3): 1-18, 2017; Article no.IRJPAC.38163
ISSN: 2231-3443, NLM ID: 101647669

A Comparative Study of Two Different Media Effect on the Electropolymerization of 2-(9-ethylcarbazol-3-yliminomethyl)phenol by Cyclic Voltammetry, Impedance Spectroscopy, XPS, UV-visible Measurements and DFT Calculation

Mounia Guergouri[1*], Rafik Bensegueni[2], Ammar Khelifa Baghdouche[1] and Leila Bencharif[1]

[1]Laboratoire de Chimie des Matériaux Constantine, Université des Frères Mentouri, Constantine 25000, Algeria.
[2]Université Mohamed Cherif Messaadia, 41000 Souk Ahras, Algérie.

Authors' contributions

This work was carried out in collaboration between all authors. Author MG designed the study, performed the statistical analysis, wrote the protocol and wrote the first draft of the manuscript. Author RB performed the theoretical calculations, managed the analyses of the study and edited the manuscript. Author AKB performed the AFM analysis and managed the literature searches. Author LB revised the manuscript critically for important intellectual content. All authors read and approved the final manuscript.

Article Information

DOI: 10.9734/IRJPAC/2017/38163
Editor(s):
(1) Surendra Reddy Punganuru, Department of Biomedical Sciences, School of Pharmacy, Texas Tech University Health Sciences Center, Amarillo, USA.
Reviewers:
(1) Yuan-Tsung Chen, National Yunlin University of Science and Technology, Taiwan.
(2) Kasem K. Kasem, Indiana University Kokomo, USA.
(3) Anukorn Phuruangrat, Prince of Songkla University, Thailand.
Complete Peer review History: http://www.sciencedomain.org/review-history/22469

Original Research Article

Received 15th November 2017
Accepted 19th December 2017
Published 27th December 2017

ABSTRACT

A carbazole-based monomer, 2-(9-ethylcarbazol-3-yliminomethyl)phenol (**SIC**), was first synthesized and characterized. It was afterward polymerized by potentiostatic methods. Oxidative polymerization of **SIC** was carried out in two media. The first one (*i.e.* Bu_4NBF_4 (0.1M)/MeCN) gives the poly(2-(9-ethylcarbazol-3-yliminomethyl)phenol). However, the second one ($LiClO_4$/MeCN + 35mM $HClO_4$), leads to another polymer, the poly(2-(9-ethylcarbazol-3-yliminomethyl)cyclohexa-2,5-diene-1,4-dione).These two novel polymers will be abbreviated here after as **PSIC** and **PDIC**,

**Corresponding author: E-mail: m.guergouri@hotmail.fr;*

respectively. If the formation of **PSIC** was expected, the formation of **PDIC** in acidic medium isn't. It was explained by a hydroxyl function oxidation of **SIC**. The obtained polymers were then characterized by cyclic voltammetry, electrochemical impedance spectroscopy, XPS, IR and UV-Vis spectroscopies. Furthermore, the corresponding electrochemical and optical bandgap values were calculated in order to get an idea about the conductive properties. The related results show that **PDIC** and **PSIC** are good conductive polymers.

Keywords: Conductive polymer; electropolymerization; cyclic voltammetry; polyimine; bandgap; DFT calculation.

1. INTRODUCTION

Electronic polymers are the subject of much research due to their reversible switch ability between insulating and conducting state. This propriety allows them to be used in several applications, such as energy storage materials and electronic devices. Among organic polymers, polycarbazoles exhibit an interesting opto-electronic and photochemical properties [1,2] due to the high electron-donating character of the carbazole ring. Owing to their proton doping [3], polycarbazole films show a fair conductivity and stable redox properties in protic medium [4].

In the present work, we investigated the electrosynthesis of a polyimine based on a carbazole unit. The monomer of this class of polymers is easily obtained. Its synthesis consists on a simple condensation between an amine and an aldehyde. We reported the electrochemical behaviour and the anodic electropolymerization of the compound 2-(9-ethylcarbazol-3-yliminomethyl)phenol (**SIC**) in two different electrolytic solutions (Bu_4NBF_4 (0.1M)/MeCN and $LiClO_4$/MeCN + 35 mM $HClO_4$).

2. EXPERIMENTAL

2.1 Materials

3-amino-9-ethylcarbazole and salicylaldehyde were obtained from *Aldrich,* and used without further purification. Tetrabutylammonium tetrafluoroborate obtained from *FLUKA*, was recrystallized in a mixture of water/methanol and dried at 100°C for 24h. Aluminium oxide was dried at 300°C under vacuum for at least 24h prior to use. The monomer (**SIC**) was prepared by condensation between 3-amino-9-ethylcarbazole and salicylaldehyde in ethanolic medium. A yellow product was obtained with a yield of 65% (m.p. 114°C).

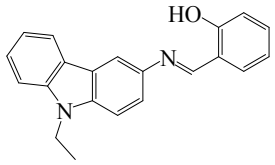

2-(9-ethylcarbazol-3-yliminomethyl)phenol (SIC)

2.2 Electrochemical Measurements

All electrochemical experiments were carried out using a computer-controlled VoltaLab PGZ 301 potentiostat/galvanostat. All data were collected and analyzed using Voltamaster software. A three-electrode cell consisting of, glassy carbon disk (GCE) as working electrode, an Ag/AgCl electrode as reference and a platinum wire as counter electrode were used. A 0.1M solution of tetrabutylammonium tetrafluoroborate (Bu_4NBF_4) in acetonitrile was used as supporting electrolyte. Anhydrous Al_2O_3 was added for drying, into the electrolytic solution. All solutions were deaerated by bubbling N_2 gas for a few minutes prior to electrochemical measurements. The potential of ferrocene/ferrocinium redox couple in the supporting electrolyte-solvent system was measured and found to be 0.435V *vs.* Ag/AgCl. Square wave parameters were pulse half-peak-to-peak ΔE_{SW} = 25mV, staircase step height ΔE_S = 5mV and scan rate v=100mV/sec. The electrochemical impedance measurements on the modified electrode were done over the frequency range from 0.1 to 100 KHz with 10mV as amplitude. For large-scale electrolysis, the working potential was controlled by a Tacussel potentiostat PRT 20-2X, and the charge consumption was measured with a Tacussel IG 6-N integrator.

2.3 Optical Measurements

UV-Vis measurements were performed on a JASCO V-660 spectrophotometer. The absorption spectra of the compounds were recorded on ITO glass transparent film (solid

phase). The infrared absorption spectra were recorded on a JASCO FT/IR-6300 spectrometer. The XPS analyses were performed with a photoelectron spectrometer ESCALAB 250 (Thermo VG).

2.4 Theoretical Calculations

Theoretical calculations were performed to estimate the energy values of the frontier molecular orbitals (HOMO and LUMO) of the studied molecules. The molecular geometries were optimized with the DFT method using the Gaussian 09 software. The used functional was B3LYP (Becke 3-parameter-Lee Yang-Parre) with the basis set of 6-311G (d,p). The figures were generated with GaussView 5.0.

3. RESULTS AND DISCUSSION

3.1 Electrochemical Polymerization of SIC in Bu_4NBF_4 (0.1M)/MeCN

The electrochemical behaviour of **SIC** was investigated on a GCE electrode by cyclic voltammetry (CV) and square wave voltammetry (SWV). Using CV, the voltammogram obtained during electrooxidation of 5×10^{-3} M of **SIC** in Bu_4NBF_4 (0.1M) / MeCN (Fig. 1), showed two peaks at 1.12 and 1.45V vs. Ag/AgCl reference electrode. These two peaks appeared also in the SWV's voltammogram at slightly lower potentials, at 1 and 1.3V, (Fig. 2). This difference in peaks potentials may be due to the high sensitivity of SWV technics [5].

The first peak probably corresponds to the oxidation of hydroxyl group which reacts easily due to the presence of *n* electrons into the oxygen atom [6]. At this potential, no polymerization of **SIC** was observed. The second peak corresponds to the formation of the radical cation of the monomer. In the cathodic scan region, **SIC** showed only one irreversible reduction peak related to the reduction of imine moiety [7].

The electrochemical polymerisation of **SIC** performed by recurrent potential scans between 0 and 1.4V in Bu_4NBF_4 (0.1M)/MeCN (Fig. 3), led to the gradual development of a new redox system centred at lower potential than the monomer (around 1.1V). The current densities of the new system increased during the successive cycles, indicating that the formed polymer film has a good adherence on the electrode [8].

3.2 Electrochemical Polymerization of SIC in $LiClO_4$ (0.1M)/MeCN in the Presence of $HClO_4$

In an acidic medium, the imine bond undergoes a protonation which commonly enhances the planarity of the polymeric material and subsequently, improves its electrical properties. A preliminary study of the **SIC** electropolymerization was carried out to specify the appropriate concentration of $HClO_4$ to add in the electrolytic solution. The current densities values at p-doping/undoping potential of **PDIC** polymer ($E_{1/2}$ = 1.02V) versus $HClO_4$ concentration (Fig. 4) showed a maximum at 35 mM. Beyond this value, the current densities decreased, proving that a stronger acid concentration would limit the growth of **PDIC** polymer [9].

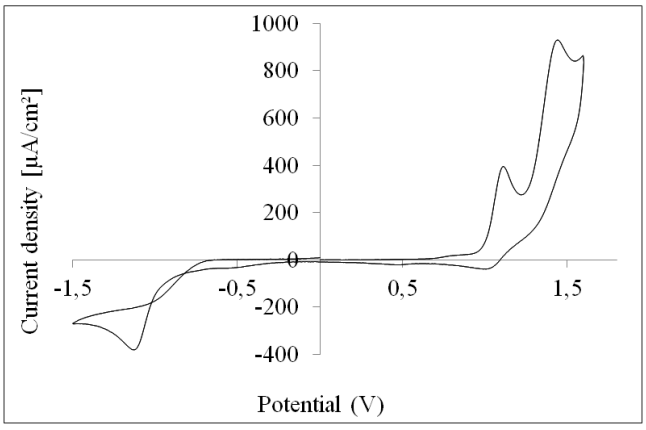

Fig. 1. Cyclic voltammogram of SIC (5×10^{-3} M) in Bu_4NBF_4 (0.1 M)/MeCN; first cycle, v = 100mV/s; working electrode: GCE; reference electrode: Ag/AgCl

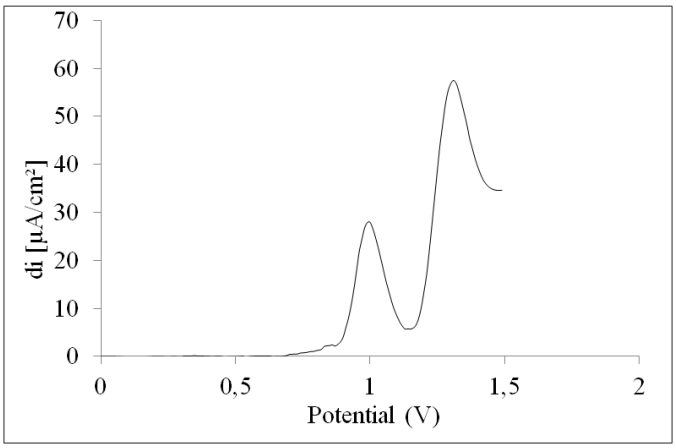

Fig. 2. Square wave voltammogram of SIC (5×10^{-3} M) in Bu_4NBF_4 (0.1 M)/MeCN; v = 100 mV/s; working electrode: GCE; reference electrode: Ag/AgCl

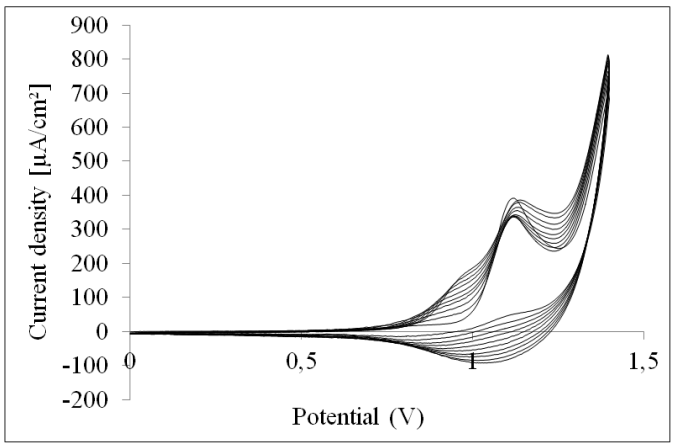

Fig. 3. Electropolymerization of SIC (5×10^{-3} M) in Bu_4NBF_4 (0.1 M)/MeCN; 10 sweeps between 0 and 1.4V; v = 100 mV/s; working electrode: GCE; reference electrode: Ag/AgCl

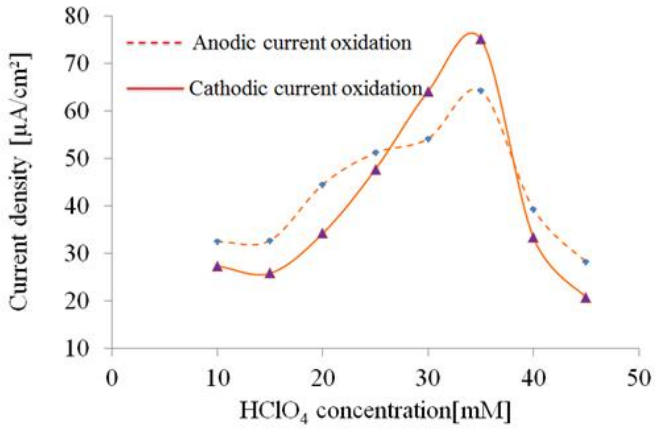

Fig. 4. Influence of $HClO_4$ concentration on current density measured at p-doping/undoping potential of PDIC. (----) Anodic current density. (—) Cathodic current density

The species mobility which increases with temperature increasing is another factor which can improve a potentiodynamic polymerization. However, this increasing is not always favourable, and can influence the electropolymerization process providing short, no-structured and less conductive chains.

Fig. 5, represents the current densities values recorded at doping-undoping potential ($E_{1/2}$ = 1.02V) versus the temperature, varied from 5 to 30°C. The anodic and cathodic currents intensities increase simultaneously and reach a maximum at 20°C. Beyond this value, the current densities decreased, and the polymer becomes less electroactive. The Fig. 6 presents the cyclic voltammogram obtained during electrooxidation of **SIC** in $LiClO_4$ (0.1M)/MeCN + 35 mM $HClO_4$. It exhibits two peaks with unequal intensities. The first one was recorded at 0.98V and was reversible, while the second one which was observed at 1.32V was irreversible. On another hand, SWV's voltammogram (Fig. 7) shows three oxidation peaks at 0.93, 1.24 and 1.44V. The first peaks, as on CV's voltammogram, was assigned to the oxidation of the hydroxyl function, while the second and third ones, combined in one peak in CV (the second peak), were related to the oxidation of imine and carbazole moieties.

The electrochemical polymerisation of **SIC** performed in protic medium (Fig. 8a) led to the growth of a new redox system centred at lower potentials (around 1.02V) comparing to the monomer. The electrochemical behaviour recoded in this medium was different from the one recorded in aprotic solvent. The oxidation of the phenol moiety in acidic medium occurs

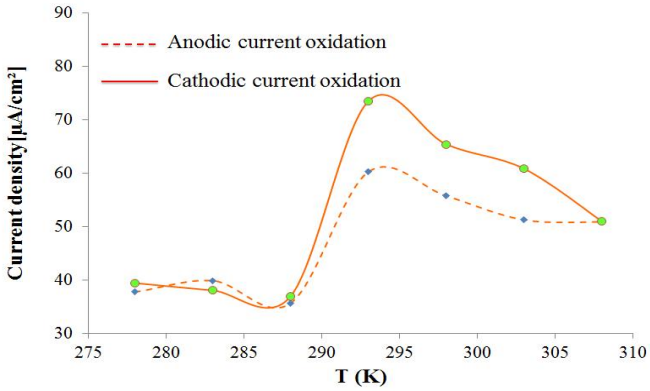

Fig. 5. Influence of temperature on current density values measured at p-doping/undoping potential of PDIC. (----) Anodic current density.(—) Cathodic current density

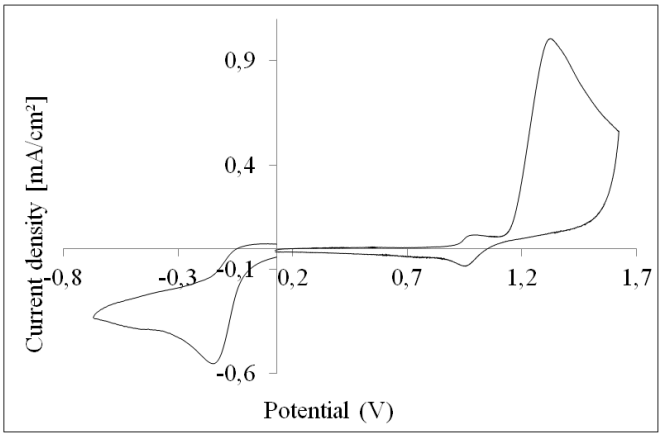

Fig. 6. Cyclic voltammogram of SIC 5×10^{-3} M in $LiClO_4$ (0.1 M)/MeCN + 35mM $HClO_4$; v = 100 mV/s; working electrode: GCE; reference electrode: Ag/AgCl

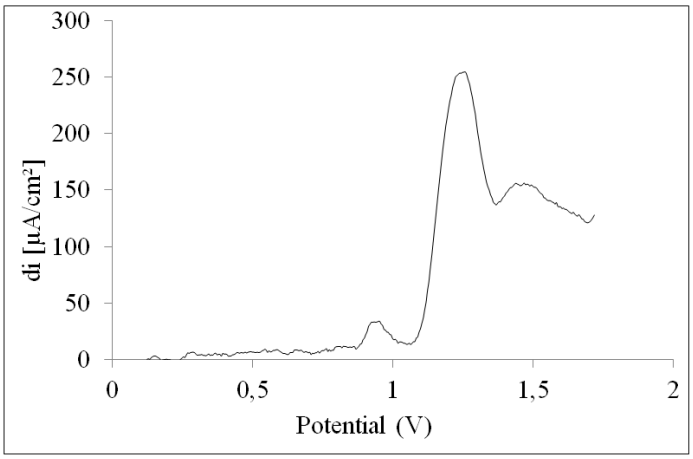

Fig. 7. Square wave voltammogram of SIC 5×10^{-3} M in $LiClO_4$ (0.1 M)/MeCN + 35 mM $HClO_4$; v = 100 mV/s; working electrode: GCE; reference electrode: Ag/AgCl

at 0.98V, and leads to its hydrolysis resulting in the formation of two products, *para*-quinone and *ortho*-quinone (Scheme 2) [6]. The both compounds showed a reversible electrochemical behavior with two electrons and two protons transfer (scheme 3) [6]. On the first negative scan (Fig. 8b), the two very weak reduction peaks recorded at 0.39 and 0.67V were attributed to the reduction of the two 2-substituted phenol oxidation products, while the peak at 0.85V corresponding to the OH oxidation. In figures 8a and 8b, E_{Red2} corresponds to the reduction of *ortho*-(2-substituted)quinone in *ortho*-(2-substituted) catechol, whereas E_{Red1} corresponds to the reduction of *para*-(2-substituted)quinone in *para*-(2-substituted)hydroquinone. On the second positive scan (Fig. 8b), two anodic peaks were recorded at E_{Ox1} = 0.5V and E_{Ox2} = 0.72V, showing the reversibility of the two reductive peaks of quinones.

Therefore, in the protic medium, the monomer (**SIC**) undergoes hydrolysis around 1V, which modifies its structure before its polymerization. This reaction which is very fast, leads to the formation of two isomers, *para*-quinone and *ortho*-quinone which oxidizes at the same potential to give **PDIC**. This fact has been confirmed by theoretical calculations. Conventionally, the oxidation potential corresponds to the required energy to remove an electron from the HOMO (Highest Occupied Molecular Orbital). Therefore, theoretical calculations showed that both isomers, *para*-quinones and *ortho*-quinones, have practically the same HOMO level values (-5.46 and -5.4eV, respectively), and a very near LUMO (Lowest Unoccupied Molecular Orbital) level values (-3.41 and -3.53eV, respectively) (Fig. 9).

Fig. 10a shows the cyclic voltammograms of **SIC** recorded between 0 and 1.3V when the scan rate varies from 0.02 to $0.5V.s^{-1}$. The anodic peak current is proportional to the square root of scan rate, most likely due to the diffusion controlled **SIC** oxidation (Fig. 10b) [10]. When increasing the scan rate, the peak potential is shifted to a more positive potentials, due to the irreversible electrode process of the oxidation reaction of **SIC** [10]. The linear variation of the anodic potential (E) against the scan rate logarithm (log v), reflecting an electrochemical-chemical mechanism (EC) involving a chemical reaction succeeding a fast electronic transfer [11].

To confirm that the nature of the compounds formed was due to the hydrolysis of hydroxyl function, a large-scale electrolysis of **SIC** at controlled potential value of 0.98V was carried out. A nacre white product was formed immediately, which once again proves the velocity of the reaction. The ^{1}HNMR spectrum (Fig. 11) of the obtained precipitate denoted DIC is in accordance with the disappearance of the OH function after oxidation. Moreover, the two peaks of phenolic ring protons recorded between 6.98 and 7.37ppm before oxidation, have moved to smaller values namely 6.3 to 6.5ppm, reflecting therefore the environment change of the corresponding protons.

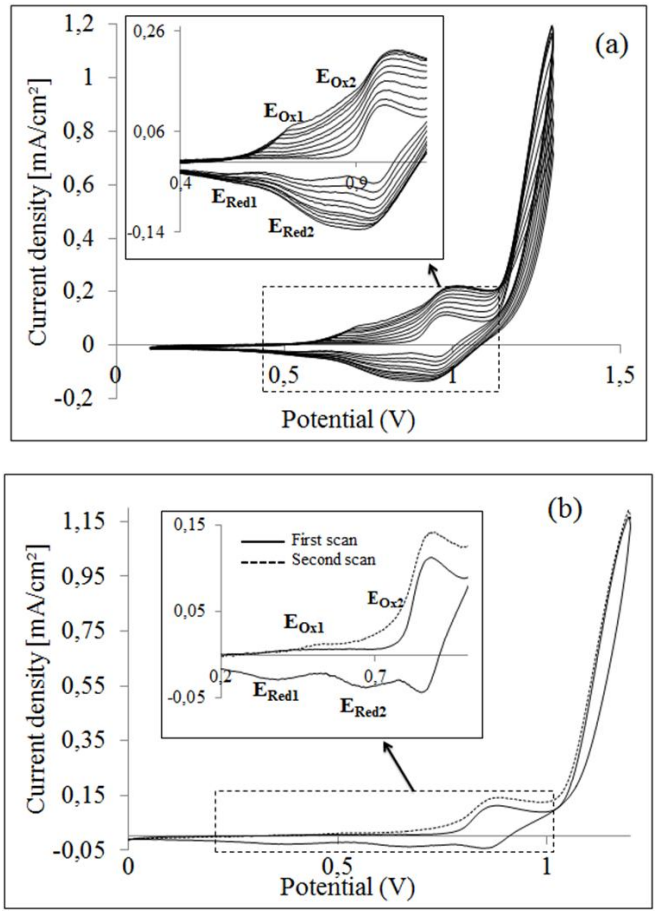

Fig. 8. Electropolymerization of SIC (5×10^{-3} M) in $LiClO_4$ (0.1 M)/MeCN + 35mM $HClO_4$; v = 100 mV/s; between 0 and 1.29 V; working electrode: GCE; reference electrode: Ag/AgCl a) 10 sweeps; b) First and second sweep

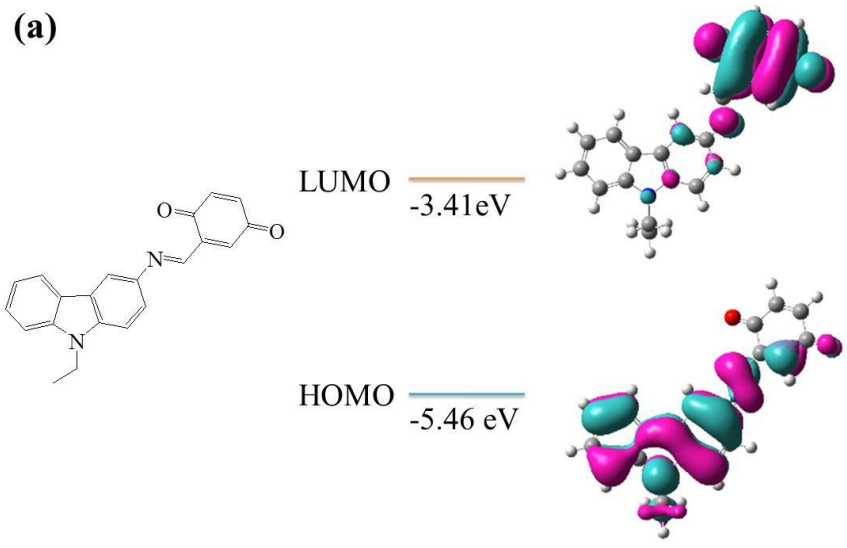

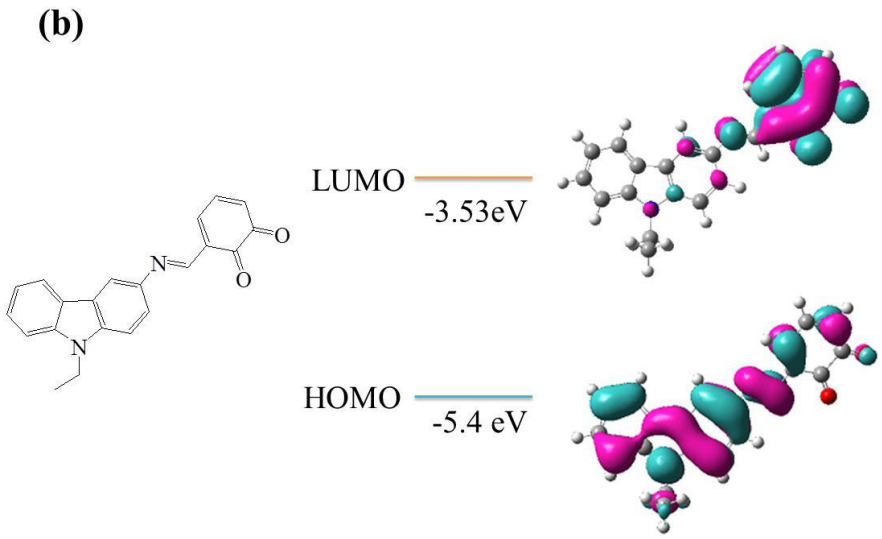

Fig. 9. Contour plots and energy values of HOMO and LUMO of (a) *para*-quinone and (b) *ortho*-quinone compounds

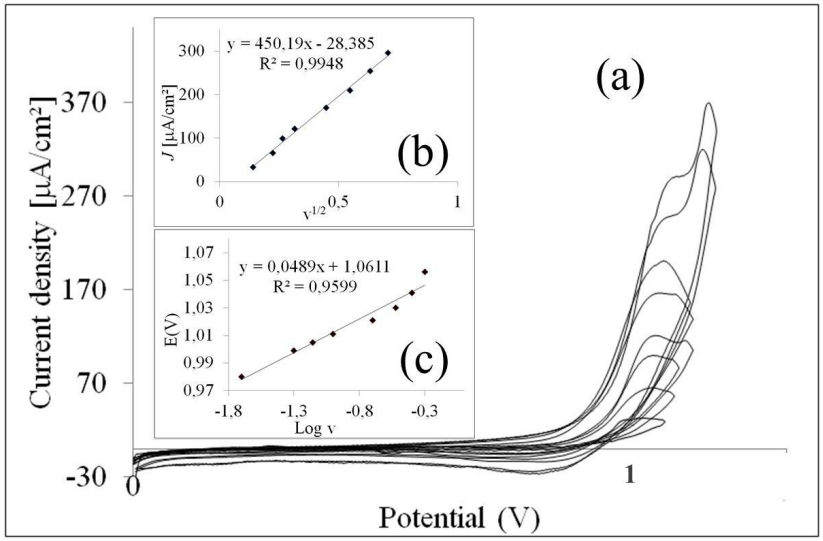

Fig. 10. (a) Cyclic voltammetric responses of 5×10^{-3} Min $LiClO_4$ (0.1 M)/MeCN + 35mM $HClO_4$ at scan rate 0.02, 0.05, 0.07, 0.1, 0.2, 0.3, 0.4, 0.5 $V.s^{-1}$. (b) The plot of peak currents vs. root of scan rate. (c) The variation of potential vs. log v

Furthermore, the color change that occurred when we dissolve **SIC** in MeCN with $LiClO_4$ (0.1M) + 35mM $HClO_4$, allowed us to think that **SIC** underwent a chemical protonation. Treated with a solution of $HClO_4$ (35mM) in MeCN, **SIC** changes its color from yellow to orange and the FTIR analysis showed the appearance of new bands (Fig. 12) of which the signal recorded at 1229 cm^{-1} was assigned to the vibration of the group $C\text{-}N^+$ [12]. Thus, we can presume that **SIC** underwent a protonation before its electropolymerization (Scheme 1).

From these data, we can say that the **SIC** monomer changes its structure in the protic medium and become a mixture of two isomers *para*-quinone and *ortho*-quinone (DIC).

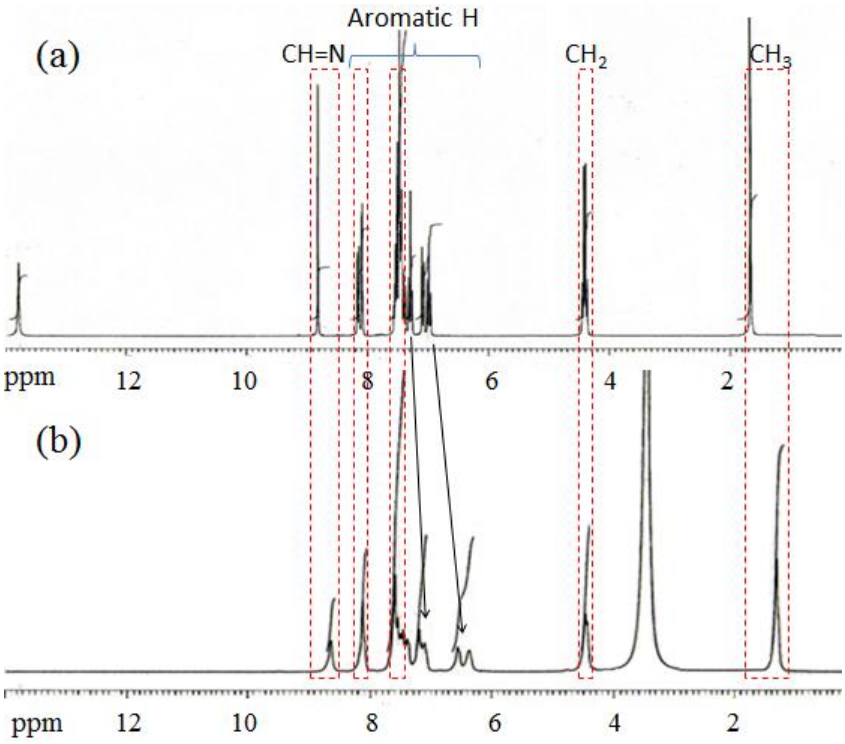

Fig. 11. ^{1}HNMR spectrum of a) SIC, b) DIC

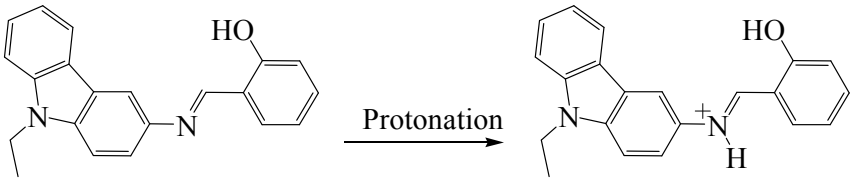

Scheme 1. Protonation of SIC

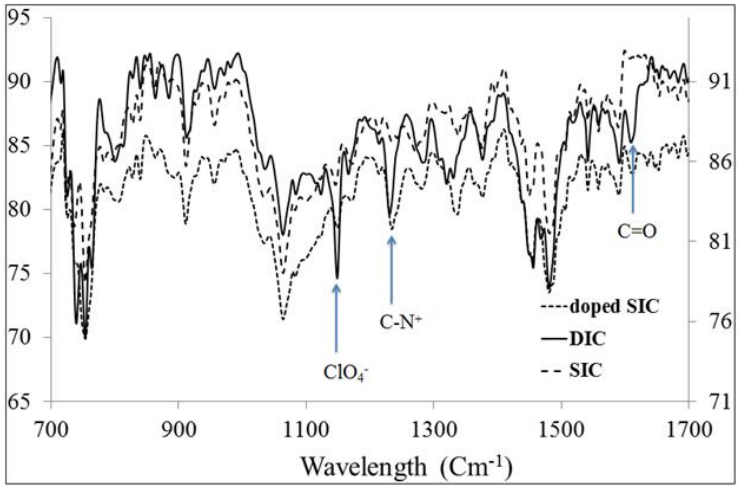

Fig. 12. IR spectra of SIC (---), DIC (—) and protoned SIC (·····)

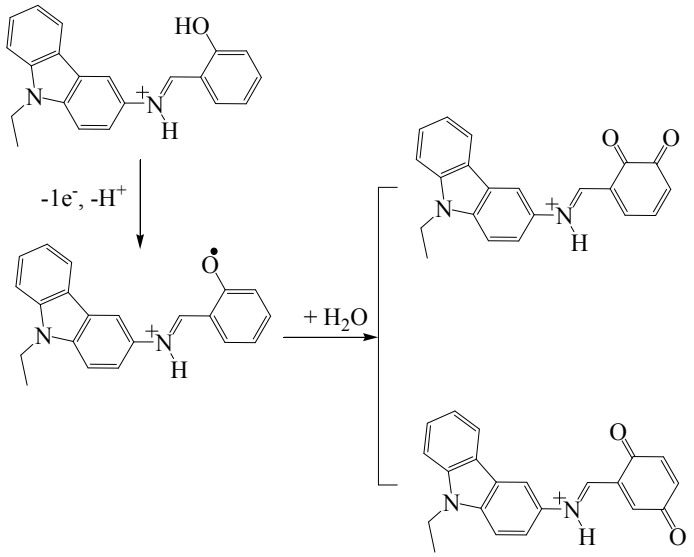

Scheme 2. First oxidation mechanism of SIC

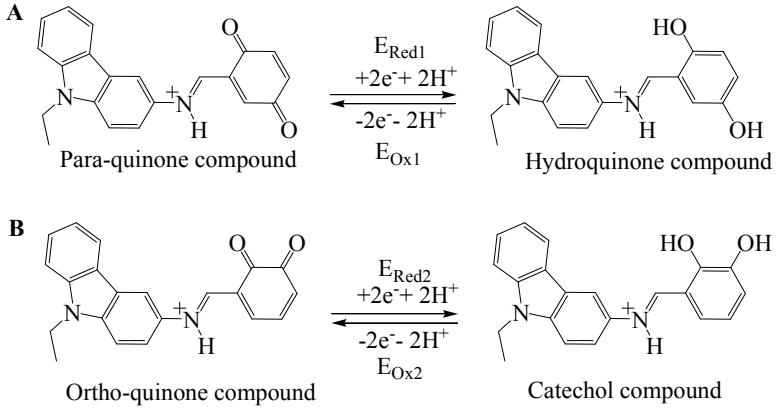

Scheme 3. Redox behaviour of: A) *Para*-quinone compound, B) *Ortho*-quinone compound

3.3 Polymers Electroactivity

The study of electrodeposited films of **PSIC** and **PDIC** polymers in both electrolytic media was done in another cell containing only the electrolytic solutions, without monomer. During the positive scans, in the two media (Fig. 13), voltammograms shows that the redox behaviour corresponds to the positive doping/undoping process, due to the participative accumulation of anionic charges, BF_4^- and ClO_4^- respectively in the polymeric matrices, pointing out the electroactive nature of the formed materials [13]. Otherwise, in the protic medium, the redox peaks appearing at $E_{1/2}$= 0.61V was related to the redox moiety of *para*-quinone / hydroquinone [6] in the polymer matrices. However, the redox system corresponding to *ortho*-quinone/catechol moiety was overlapped with the one of **PDIC**. The electrochemical behaviours of **PSIC** and **PDIC** affirm the difference between their structures.

The thin layer film of both polymers was analyzed by XPS, a much more sensitive measurement than IR. The XPS spectra of the two polymers coated ITO, are represented on Fig. 14. Either for **PSIC** or **PDIC**, the band at 399.9eV corresponds to the N_{1s} signal, while the one at 532.5eV corresponds to the signal of O_{1s} [14]. In the spectrum of **PSIC**, there are two bands in the C region (Fig. 15), corresponding to C-C (284.7eV) and C-OH (286.5eV) [15]. However, in the spectrum of **PDIC**, we have the band of the C-C at 284.7eV, accompanied by another one at 288.2eV corresponding to the C=O energy (Fig. 16) [16].

3.4 Electrochemical Impedance Measurements (EIS)

The electrochemical impedance spectroscopy permits to understand the charge transport mechanism of electrolyte ions during the redox reaction. Several works have been focused on the mass transport in conducting polymers. However, due to the complexity of these phenomena, their complete understanding is not achieved yet. The impedance measurements were conducted at a potential corresponding to the oxidation state of each polymer (around 1V) while varying the frequency from 0.1 to 100 kHz. From the impedance response, the thin film coated electrode can be represented from electrical point of view by a Randles-type equivalent circuit [17].

Fig. 17a shows the nyquist plot of **PDIC** coated GCE in $LiClO_4$ (0.1 M)/MeCN + 35mM $HClO_4$, while Fig. 17b shows **PSIC** coated GCE in Bu_4NBF_4 (0.1 M)/MeCN. For **PDIC** coated GCE, there is three characteristic parts of the diagram. At high frequencies, a semicircle characteristic for a charge transfer in polymer bulk is observed, and represented in equivalent circuit by parallel combination of film resistance R_{Bulk} and capacitance C_{Bulk} in series with solution resistance R_e [18]. At intermediate frequencies, a beginning of a second semicircle is recorded. The impedance response depends on the shapes of pores in the surface (theory of porous electrodes developed by *de LEVIE*) [19]. The more the pore is easily accessible, the more the semicircle tends to disappear and to be replaced by a straight line. Compared to the first one, the second semicircle is flattened, because the film-electrolyte interface is not smooth and uniform [20]. Consequently, the double layer capacitance in the equivalent circuits is replaced by a constant phase element (CPE) [20]. The impedance response is represented in equivalent circuit, by a parallel combination of charge transfer resistance R_{ct} (between film and solution) and pseudo-capacitive charging of the film CPE_1 [18]. At low frequencies, a straight line representing Warburg-type impedance due to a finite diffusion of counter-ions species within the film is observed. This line is recorded with a slope $\theta \neq 45°$, as often found in the presence of inhomogeneities in a coated material, or under non-uniform diffusion conditions [21].

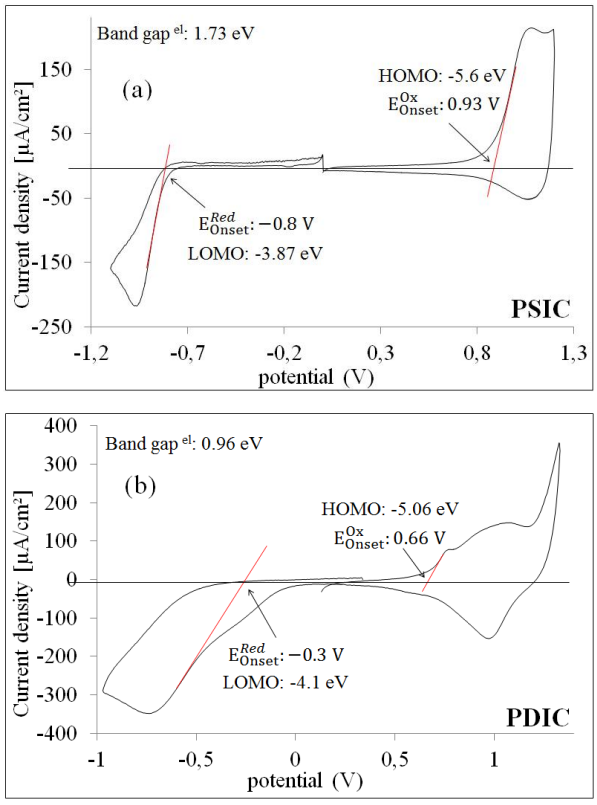

Fig. 13. Cyclic voltammograms for oxidation of: a) PSIC coated GCE in Bu_4NBF_4 (0.1 M)/MeCN; b) PDIC coated GCE in $LiClO_4$ (0.1 M)/MeCN + 35 mM $HClO_4$. v = 100mV/s

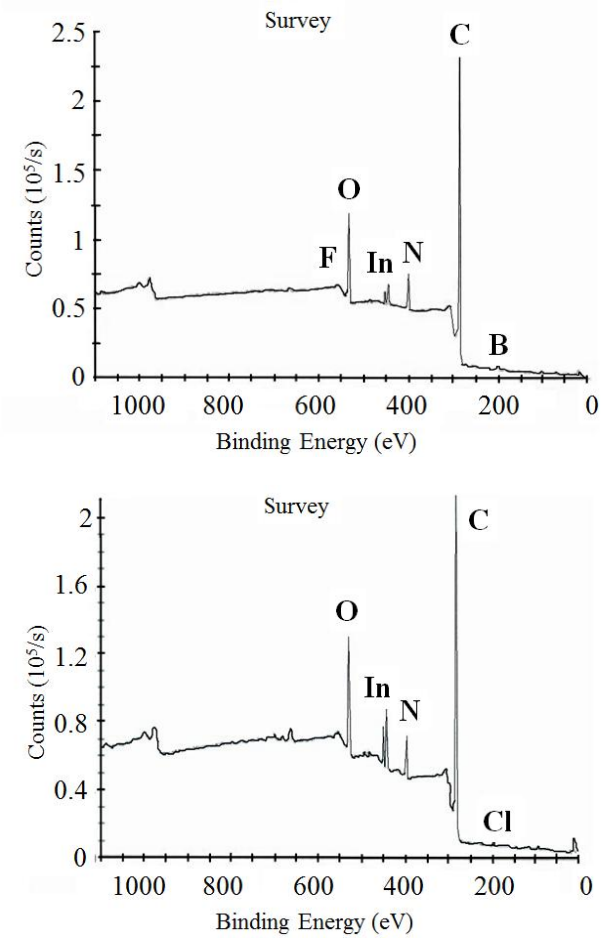

Fig. 14. Survey spectra of: a) PSIC coated ITO, b) PDIC coated ITO

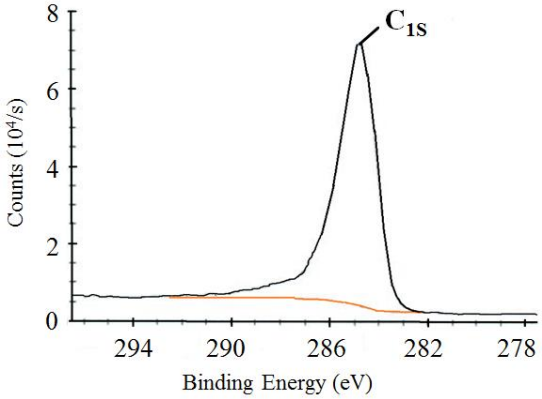

Fig. 15. Survey spectra of PSIC coated ITO

For the **PSIC** coated GCE, the diagram showed only a beginning of a semicircle, characteristic for a charge transfer between polymer and solution, and represented in equivalent circuit by parallel combination of the charge transfer resistance R_{ct} and the interfacial capacitance of the film C_{dl}. Thus, there is a pure charge transfer control and no diffusion limitations [22,23].

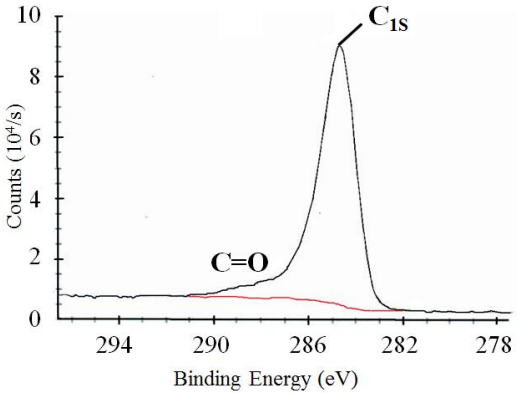

Fig. 16. Survey spectra of PDIC coated ITO

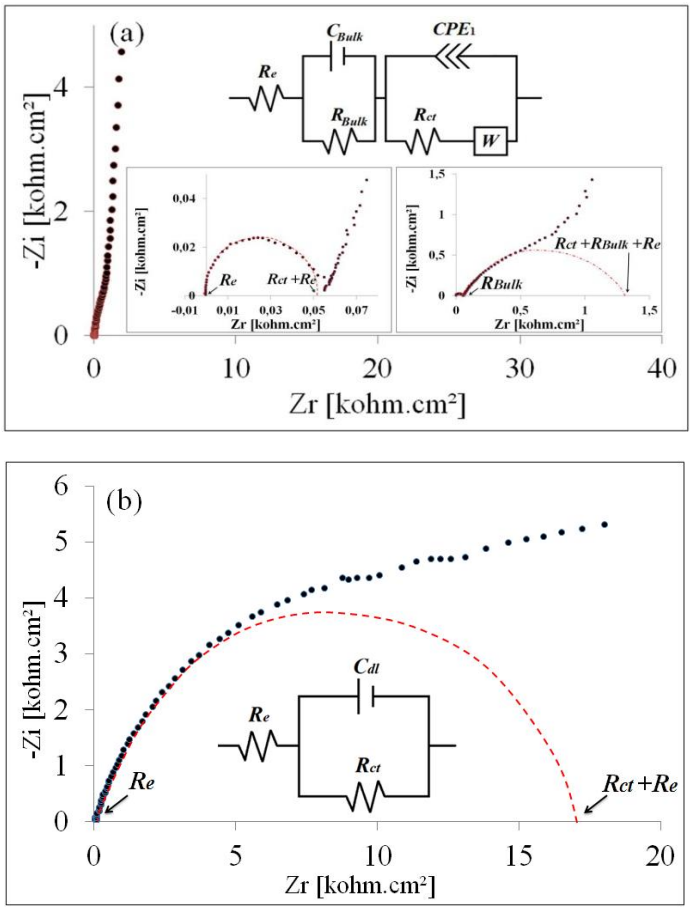

Fig. 17. Nyquist plots and Randles-type equivalent circuits of: a) PDIC, b) PSIC

The charge transfer resistance recorded for **PDIC** film was much lower than the one recorded for **PSIC** film, which implies that **PDIC** is more conductive than **PSIC** [24].

3.5 Optical and Electrochemical Bandgap

The electrical properties of conjugated polymers depend on their structures and on the delocalization of π electrons that is related to the

planarity of the chain. Thus, due to its protonated state, **PDIC** would be more planar than **PSIC** and then, would exhibit better electrical properties.

Otherwise, the bandgap is another important factor determining the electrical conductivity. The bandgap can be measured in two different ways, electronic bandgap determined from cyclic voltammetry and optical bandgap estimated from UV-Visible spectroscopy.

By cyclic voltammetry, HOMO and LUMO energy levels could be estimated from the onsets of oxidation and reduction potentials, respectively, according to the following equations [25]:

$$E_{HOMO}\ (eV) = -\ [E^{ox}_{onset} + 4.4]$$
$$E_{LUMO}\ (eV) = -\ [(E^{red}_{onset} + 4.4]$$

The difference between HOMO and LUMO energies, give the electrochemical bandgap value (E_g^{el}). The obtained results were presented in Fig. 13a and 13b and summarized in Table 1.

The electrochemical bandgap recorded for **PDIC** is very smaller than the one recorded for **PSIC** (0.96 and 1.73eV, respectively). This value which reflects the conductivity of the material was related to the doping level. Indeed, when a polymer is oxidized, by analogy of the admitted results, an electron is removed from the HOMO and a positive polaron or radical cation is created. The energy level associated with that positive polaron, partially relocated on monomer units of the polymer chain, is represented by a destabilized bonding orbital of which the energy is higher than that of the HOMO. Furthermore, the protonation of imine moiety, which was preferably compared with that of the amine sites [26], increases planarity of polyazometines [27], which decreases the LUMO level and increases the HOMO level. Subsequently, the bandgap is decreased. Hence, it is clear that in the medium containing $LiClO_4$ (0.1M) / MeCN + 35mM $HClO_4$, **PDIC** underwent protonation and electrochemical doping, which can explain its low energy bandgap.

Optical properties of the polymer films on ITO glass were observed by recording the changes in the absorption spectra under voltage at 0 and 1V. The electronic absorption of neutral films exhibit an absorption band around 355 and 305 nm for **PSIC** and **PDIC**, respectively. These bands which were due to a $\pi \rightarrow \pi^*$ transition lose intensity, during oxidation.

Polarized at 1V in $LiClO_4$ (0.1M)/MeCN/$HClO_4$ (35mM), **PDIC** thin layer presents a modification in the optical spectrum with the appearance of a broad band around 605nm (Fig. 18). In a similar way, when **PSIC** thin layer is polarized at 1V, the optical spectrum shows a new absorption band at 477nm (Fig. 19).

The optical bandgap is calculated according to $E_g^{opt} = 1240/\lambda_{onset}$, where λ_{onset} is obtained from the intersection between the baseline and the tangent of the UV-Vis band-end [25].

The optical bandgap of **PDIC** (1.51eV) is lower than that of **PSIC** (1.99eV). The bandgap value can be affected by several factors such as an intra-chain charge transfer and substituents effect [28]. Fig. 21 shows the (DFT) theoretical calculation for the distributions of the frontier molecular orbitals of **SIC**. Compared to **SIC**,

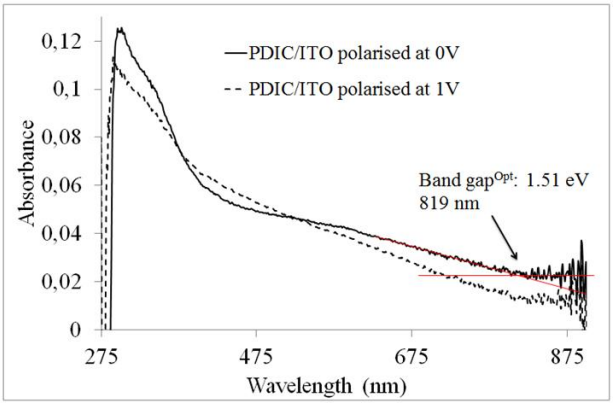

Fig. 18. The absorbance versus the wavelength registered with PDIC coated ITO polarized in the $LiClO_4$ (0.1M) / MeCN + (35mM) $HClO_4$, at: 0V (—) and 1V (- - -)

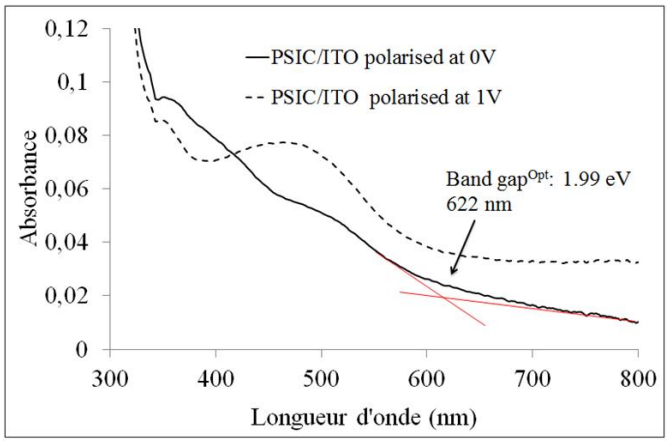

Fig. 19. The absorbance versus the wavelength registered with PSIC coated ITO polarized in the $LiClO_4$ (0.1M) / MeCN + (35 mM) $HClO_4$ at: 0V (—) and 1V (- - -)

Table 1. Electrochemical and optical bandgaps

	E^{ox}_{onset} (vs. Ag/AgCl)[a]	E^{red}_{onset} (vs. Ag/AgCl)[a]	E_{HOMO} (eV)	E_{LUMO} (eV)	E_g^{el} (eV)[b]	E_g^{opt} (eV)[c]
SIC	1.20	-0.96	-5.87	-3.71	2.16	2.84
PSIC	0.93	-0.80	-5.60	-3.87	1.73	1.99
DIC	1.14	-0.01	-5.54	-4.39	1.15	- - - -
PDIC	0.66	-0.30	-5.06	-4.10	0.96	1.51

a The onset potentials are determined from the intersection of the two tangents drawn at the rising current and the baseline charging current of the CV traces . b Energy of the bandgap is calculated from the difference between the energy of the HOMO and the LUMO. c The optical bandgap is calculated according to $E_g^{opt} = 1240/\lambda_{onset}$

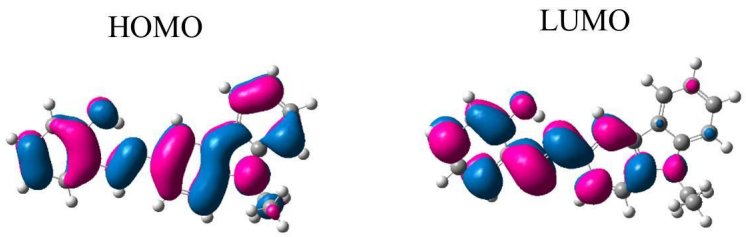

Fig. 20. The contour plots and energy values of HOMO and LUMO orbitals of SIC

para-quinone and *ortho*-quinone compounds are formally donor-acceptor (D-A) type moieties (Fig. 9). Phenol oxidation in **SIC** leads to an electronic deficient state of the quinone moiety of the formed molecules (*para*-quinone and *ortho*-quinone), while their carbazole moieties are electrons donor. Indeed, in a D-A system, a charge transfer for the donor to the acceptor increases the length of the π-system through resonance. The increasing in the conjugation length of a molecule causes the decrease of its bandgap [29].

The difference in the surface topography was observed by the atomic force microscopy working in the contact mode (Fig. 21). The 3D view shows that there are numerous smaller surface undulations with a precipitation of different shapes [30]. However, we notice that precipitations in **PDIC** are not as numerous as in **PSIC** thin film.

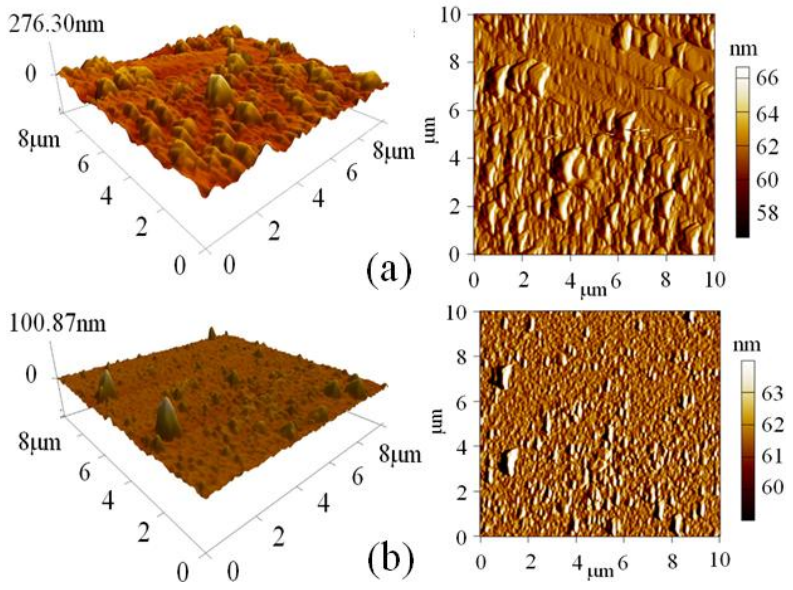

Fig. 21. AFM image of: a) PSIC thin layer, b) PDIC thin layer

4. CONCLUSION

The electrochemical polymerisation of **SIC** is performed in both protic and organic medium. During the anodic oxidation in protic medium containing $LiClO_4$/MeCN + (35mM) $HClO_4$, **SIC** undergoes hydrolysis around 1V, which modifies its structure before its polymerization. This reaction is very fast, and leads to the formation of two isomers, *para*-quinone and *ortho*-quinone (**DIC**) which oxidizes at the same potential and form **PDIC**. In the organic medium, the **SIC** retains its initial structure, and leads after oxidation to the corresponding polymer **PSIC**. The electrochemical behaviour of **PSIC** and **PDIC** supports the conductive character of both polymers and the difference between their structures. In an acidic medium, the imine bond undergoes a protonation which increases commonly the planarity of the polymeric material and subsequently, improves its electrical properties. The charge transfer resistance recorded for the **PDIC** film was much lower than the one recorded for the **PSIC** film. The electrochemical and the optical bandgaps of **PDIC** are lower than those of **PSIC**. The difference in structures of both polymers could explain these results. Compared to **SIC**, *para*-quinone and *ortho*-quinone compounds are formally electrons donor-acceptor (D-A) type moieties. In a D-A system, a charge transfer from the donor to the acceptor increases conjugation length through resonance which causes the decrease of its bandgap. Therefore, these findings indicate that **PDIC** is more conductive than **PSIC**.

COMPETING INTERESTS

Authors have declared that no competing interests exist.

REFERENCES

1. Madhavan S, Santhanam KSV. Structurally modified polymer of carbazole with specific catalysis in electrooxidation of organic molecules. Mol. Cryst. Liq. Cryst. Inc. Nonlinear Opt. 1988;160(1):111.
2. Itaya A, Yamamoto K, Masuhara H, Kimizuka N, Kunitake T. Laser-induced geometrical change of fluorescent traps in cast films of carbazole-containing bilayer membranes. Thin Solid Films. 1991; 202(1):137.
3. Verghese MM, Basu T, Malhotra BD. Influence of pH on the electroactivity of polycarbazole. Mater. Sci. Eng. C. 1995;3: 215.
4. Grazulevicius JV, Strohrieglb P, Pielichowskic J, Pielichowski K. Carbazole-containing polymers: Synthesis, properties and applications. Prog. Poly. Scien. 2003;28(9):1297.
5. Lovrić M, Komorsky-Lovric Š. Square-wave voltammetry of an adsorbed reactant. J. Electroanal. Chem. Interfacial Electrochem. 1988;248(2):239.

6. Enache TA, Oliveira-Brett AM. Phenol and Para-substituted phenols electrochemical oxidation pathways. J. Electroanal. Chem. 2011;655:9.
7. Beginn C, Gražulevičius JV, Strohriegl P, Simmerer J, Haarer D. Synthesis of poly(9-hexyl-3,6-carbazol-yleneethynylene) and its model compounds. Macromol. Chem. Phys. 1994;195(7):2353.
8. Hu B, Lv X, Sun J, Bian G, Ouyang M, Fu Z, Wang P, Zhang C. Effects on the electrochemical and electrochromic properties of 3,6 linked polycarbazole derivative by the introduction of different acceptor groups and copolymerization. Org. Electron. 2013;14(6):1521.
9. Benachenhou F, Mimouni N, Mederbel Y, Kaïd-Slimane R. Hydrolysis study: Synthesis of novel styrenic Schiff bases derived from benzothiazole. Arab. J. Chem. 2012;5(2):245.
10. Fotouhi L, Fatollahzadeh M, Heravi MM. Electrochemical behavior and voltammetric determination of sulfaguanidine at a glassy carbon electrode modified with a multi-walled carbon nanotube. Int. J. Electrochem. Sci. 2012;7:3919.
11. Haj-Said A, Matoussi M'halla F, Roudesli S. L'oxydation anodique du paraéthylanisole dans l'acétonitrile sur électrode de platine: Etude mécanistique et préparative. J. Soc. Chim. Tun. 2010; 12:151.
12. Nahar MS, Zhang J. Charge transfer in anion doped polyaniline. 2011 International Conference on Signal, Image Processing and application IPCSIT. 2011; 21:216.
13. Pérez Guarìn SA, Skene WG. Thermal, photophysical, and electrochemical characterization of a conjugated polyazomethine prepared by anodic electropolymerization of a thiophenoazomethine co-monomer. Mater. Lett. 2007;61(29):5102.
14. Volkov A, Tourillon G, Lacaze PC, Dubois JE. Electrochemical polymerization of aromatic-amines-IR, XPS and PMT study of thin-film formation on a Pt electrode. J. Electroanal. Chem. 1980;115: 279.
15. Akhter S, Zhou XL, White JM. XPS study of polymer/organometallic interaction: Trimethyl aluminum on polyvinyl alcohol polymer. Surface Applied Science. 1989; 37(2):201.
16. González-Domínguez JM, Castell P, Bespin-Gascón S, Ansón-Casaos A, Díez-Pascual A, Gómez-Fatou MA, Benito AM, Maser WK, Martínez M. Covalent functionalization of MWCNTs with poly(p-phenylene sulphide) oligomers: A route to the efficient integration through a chemical approach. J. Mater. Chem. 2012;22: 21285.
17. Randles JEB. Kinetics of rapid electrode reactions. Discuss. Faraday Soc. 1947;1: 11.
18. Rubinstein I, Sabatani E, Rishpon J. Electrochemical impedance analysis of polyaniline films on electrodes. J. Electrochem. Soc. 1987;134:3078.
19. Keiser H, Beccu KD, Gutjahr MA. Abschätzung der porenstruktur poröser elektroden aus impedanzmessungen. Electrochim. Acta. 1976;21:539.
20. Tiginyanu I, et al. (ed.). Nanostructures and thin films for multifunctional applications, NanoScience and Technology, Springer International Publishing Switzerland; 2016.
21. Macdonald JR, (ed.). Impedance Spectroscopy, Wiley, New York; 1987.
22. Grundmeier G, Schmidt W, Stratmann M. Corrosion protection by organic coatings: Electrochemical mechanism and novel methods of investigation. Electrochimica Acta. 2000;45:2515.
23. Mostany J, Sharifker BR. Impedance spectroscopy of undoped, doped and overoxidized polypyrrole films. Synthetic Metals. 1997;87:179.
24. Ehsani A, Babaei F, Mostaanzadeh H. Electrochemical and optical investigation of conductive polymer and MWCNT nanocomposite film. J. Braz. Chem. Soc. 2015;26(2):331.
25. Khelifa Baghdouche A, Guergouri M, Mosbah S, Benmekhbi L, Bencharif L. The synthesis, physicochemical properties and electrochemical polymerization of fluorene-based derivatives as precursors for conjugated polymers. Tetrahedron Lett. 2015;56(20):2574.
26. Macdiarmid AG, Chiang JC, Halpern M, Huang WS, Mu SL, Nanaxakkara LD, Wu SW, Yaniger SI. "Polyaniline": Interconversion of metallic and insulating forms. Mol. Cryst. Liq. Cryst. 1985; 121(1-4):173.

27. Yang CJ, Jenekhe SA. Conjugated aromatic polyimines. 2. synthesis, structure, and properties of new aromatic polyazomethines. Macromolecules. 1995; 28:1180.
28. Winder C, Sariciftci NS. Low bandgap polymers for photon harvesting in bulk heterojunction solar cells. J. Mater. Chem. 2004;14:1077.
29. Pavia DL, Lampman GM, Kriz GS. Introduction to spectroscopy. 2nd Ed., Saunders College Publishing; 1996.
30. Weszka J, Szindler M, Śliwa A, Hajduk B, Jurusik J. Reconstruction of thin films polyazomethine based on microscopic images. Archives of Materials Science and Engineering. 2011;48:40.

Peer-review history:
The peer review history for this paper can be accessed here:
http://sciencedomain.org/review-history/22469